



**HAL**  
open science

**Combined effect between PVP and glass wool for improvement of the photocatalytic activity under visible light of bismuth (III) oxyhalide and access to  $\alpha$ -Bi<sub>2</sub>O<sub>3</sub>-BiOI-BiOBr**

Meriem Mansour, Imane Benyamina, Bahia Benalioua, Abdelhadi Bentouami, Bruno Boury, Hafida Hentit, Pierre-Emmanuel Lippens

► **To cite this version:**

Meriem Mansour, Imane Benyamina, Bahia Benalioua, Abdelhadi Bentouami, Bruno Boury, et al.. Combined effect between PVP and glass wool for improvement of the photocatalytic activity under visible light of bismuth (III) oxyhalide and access to  $\alpha$ -Bi<sub>2</sub>O<sub>3</sub>-BiOI-BiOBr. Applied Surface Science, 2020, 534, pp.147577. 10.1016/j.apsusc.2020.147577 . hal-03084804

**HAL Id: hal-03084804**

**<https://hal.science/hal-03084804>**

Submitted on 21 Dec 2020

**HAL** is a multi-disciplinary open access archive for the deposit and dissemination of scientific research documents, whether they are published or not. The documents may come from teaching and research institutions in France or abroad, or from public or private research centers.

L'archive ouverte pluridisciplinaire **HAL**, est destinée au dépôt et à la diffusion de documents scientifiques de niveau recherche, publiés ou non, émanant des établissements d'enseignement et de recherche français ou étrangers, des laboratoires publics ou privés.



# Combined effect between PVP and glass wool for improvement of the photocatalytic activity under visible light of bismuth (III) oxyhalide and access to $\alpha$ -Bi<sub>2</sub>O<sub>3</sub>-BiOI-BiOBr

Meriem Mansour<sup>a</sup>, Imane Benyamina<sup>a</sup>, Bahia Benalioua<sup>a</sup>, Abdelhadi Bentouami PhD<sup>a</sup>, Bruno Boury PhD<sup>b</sup>, Hafida Hentit<sup>a</sup>, Pierre-Emmanuel Lippens<sup>c</sup>

<sup>a</sup> Laboratoire de Valorisation des Matériaux, Université Abdelhamid Ibn Badis de Mostaganem, BP 227, Mostaganem 27000 Algeria

<sup>b</sup> ICGM-CMOS-UMR 5253, Université de Montpellier CC 1701, Place Eugène Bataillon, 34095 Montpellier Cedex 05, France

<sup>c</sup> ICGM-AIME-UMR 5253, Université de Montpellier CC 1502, Place Eugène Bataillon, 34095 Montpellier Cedex 05, France

## ARTICLE INFO

### Keywords

Hetero-composite  
Semiconductors  
Photodegradation  
RhB  
Bismuth oxyhalides

## ABSTRACT

Improvement of the photocatalytic efficiency of BiOI/BiOBr composite have been obtained by a combined effect between a structuring agent like polyvinylpyrrolidone (PVP) and glass wool (GW) introduced during their synthesis by solvothermal (STP) or hydrothermal (HTP) process. The photocatalysts were characterized by XRD, SEM, XPS, UV-Visible DRS, BET and EDX and their activity tested in the photo-degradation of Rhodamine B (RhB) under visible light. Photocatalyst prepared by STP have higher photocatalytic efficiency than those prepared by HTP, moreover, the presence of PVP and GW greatly improve this efficiency, a total discoloration of RhB solution (20 mg L<sup>-1</sup>) being obtained after 18 min. The photodegradation mechanism has been proposed by the identification of the radical species responsible for the degradation. Indeed, two radical species have been identified for the catalyst prepared without GW, most of them the hole ( $h^+$ ) and moderately super oxide anion ( $O_2^{\cdot-}$ ). Differently, for the catalyst prepared with GW, three species have been identified,  $h^+$  being the main species with a moderate contribution of the hydroxyl radical ( $HO^{\cdot}$ ) and  $O_2^{\cdot-}$ .

## 1. Introduction

Knowing that visible light accounts for about 44% of the solar spectrum, the future of photocatalysis relies on efficient and stable photocatalyst under visible light and has already succeeded in many works [1–7]. Photocatalysts with photocatalytic efficiency under visible light are narrow-band gap semiconductors [8], among them bismuth oxyhalides (BiOX), in particular BiOBr and BiOI. The latter, separately, present photocatalytic efficiency under visible light higher than other conventional semiconductors [9–11]. Moreover, the combination of these two bismuth oxyhalides in adequate proportions can lead to higher photocatalytic activity for the assembly of these hetero-structural compounds at different molar ratios between bromine and iodine [11–13]. Additional improvement can be obtained by combining BiOI-BiOBr with other photoactive materials such as graphitic carbon nitride [14,15], graphene oxide [16,17], reduced graphene oxide [18] iron oxide [13], these providing better electron-hole separation, preventing recombination and increasing their efficiency compared to the bismuth oxyhalide mixture alone.

Like for any catalytic process, the efficiency of the photocatalyst also depends on one hand on textural parameters such as specific sur-

face area, pore volume, and pore diameter and on the other hand on structural parameters like crystallinity, crystal size and defect [19–21]. In order to optimize these parameters, two synthesis pathways are generally chosen, hydrothermal and solvothermal, the latter being frequently reported to further improves the efficiency and photocatalytic stability compared to the hydrothermal method [22,23]. Besides, supporting the photocatalyst is now an additional issue pursuing different objectives like (i) avoiding the release of nano-to-macro- particles in relation with environmental issues, (ii) limiting the quantity of material to a thin coated layer on the support, (iii) increasing the efficiency through photocatalyst/support interactions or/and (iv) allowing a faster mass transport due to separation between the particles at the surface. Indeed, the use of fibers such as carbon fibers as a supporting of BiOX lead to improved photocatalytic efficiency compared to photocatalyst alone [24–27]. In addition, other fibers without optical proprieties have also been tested as a support for bismuth oxyhalide such as luffa fiber [28], Al<sub>2</sub>O<sub>3</sub>-based ceramic fibers [29,30], glass fiber cloth [31] and cellulose fiber [32]. The combination between the semiconductor and an optically inactive support sometimes contributes to improve the adsorption and photocatalytic degradation of the pollutant.

Yes

E-mail addresses: [abdelhadi.bentouami@univ-mosta.dz](mailto:abdelhadi.bentouami@univ-mosta.dz) (A. Bentouami); [bruno.boury@umontpellier.fr](mailto:bruno.boury@umontpellier.fr) (B. Boury)

<https://doi.org/10.1016/j.apsusc.2020.147577>

Received 22 July 2020; Received in revised form 6 August 2020; Accepted 12 August 2020

Available online xxx

0169-4332/© 2020.

In one of our recent work, we demonstrated that the presence of glass wool (GW) at 2 w% increases by 40% the efficiency of a nano-to-macro photocatalyst,  $\text{Bi}_2\text{O}_3\text{-ZnO}$ . So far, most of the increase of the efficiency is ascribed to an increase of the textural parameters of  $\text{Bi}_2\text{O}_3\text{-ZnO}$  resulting from the presence of the GW. However, how this optically transparent but inactive support impact the texture of  $\text{Bi}_2\text{O}_3\text{-ZnO}$  and how GW interact with  $\text{Bi}_2\text{O}_3\text{-ZnO}$  in the photocatalytic process are two important features still open to discussion [22].

These results have prompted us to investigate the possibility to improve the photocatalytic activity of  $\text{BiOI/BiOBr}$  composite by a similar way, using GW as a cheap, non-toxic and chemically stable fibrous support and transparent to visible light, a decisive point in the case of  $\text{BiOI/BiOBr}$  composite. Besides, it has been reported that polyvinylpyrrolidone (PVP), a water-soluble surfactant, acts as a structuring agent in the synthesis of  $\text{BiOX}$  leading to different morphologies and improvement of the photocatalytic efficiency [33–37]. Based on this, we considered interesting to explore the association and eventually the combined effect between GW and PVP to improve the bismuth mixed-oxyhalides photocatalysts prepared either by hydrothermal (HTP) or solvothermal (STP) method. To our best knowledge, this has never been disclosed before, neither the use of GW, nor its association with PVP.

The obtained materials were tested in the photo-degradation of Rhodamine B (RhB) under visible light and compared to other photocatalyst. Although different “model” of pollutant may be more accurate, RhB is a classical dye that allows comparison with previous studies. In this report we also performed identification of the photoactive species and found important differences related to the presence of GW that modifies the textural parameter and the composition of the photocatalyst.

In preliminary assays reported in Supplementary Information (S.I), the effects of GW and of the structuring agent PVP were extensively studied with respect of the molar ratio  $\text{Bi}/(\text{Br} + \text{I}) = 1$  and variation of the molar fraction of Br  $x_{\text{Br}}$  ( $x_{\text{Br}} = n_{\text{Br}}/(n_{\text{Br}} + n_{\text{I}})$ ) and I  $x_{\text{I}}$  ( $x_{\text{I}} = n_{\text{I}}/(n_{\text{Br}} + n_{\text{I}})$ ). We only present here the materials with the optimal molar fraction of Br and I:  $x_{\text{Br}} = 0.75$  and  $x_{\text{I}} = 0.25$ . As fre-

quently reported in the literature [38,39], here also this composition lead to the best results by photo-discoloration of the RhB solution.

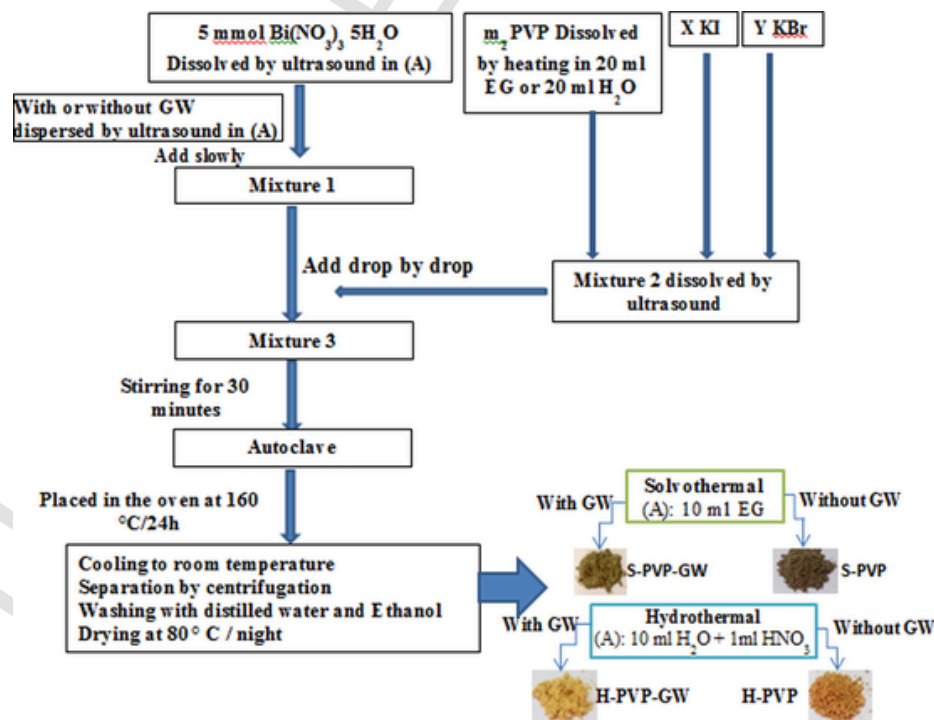
## 2. Experimental

### 2.1. Photocatalysts synthesis

All starting chemicals of analytical purity Potassium Bromide (KBr); Potassium Iodine (KI); Bismuth(III) nitrate pentahydrate ( $\text{Bi}(\text{NO}_3)_3 \cdot 5\text{H}_2\text{O}$ ); Sodium Hydroxide (NaOH); Ethylene Glycol ( $\text{C}_2\text{H}_6\text{O}_2$ ) (EG), Ethanol ( $\text{C}_2\text{H}_5\text{OH}$ ), Nitric acid ( $\text{HNO}_3$ ), PolyVinylPyrrolidone with a molecular weight of 360,000 g/mol (PVP 360), Ethylene di-amine tetra acetic acid disodium salt dehydrate  $\text{C}_{10}\text{H}_{14}\text{N}_2\text{Na}_2\text{O}_8 \cdot 2\text{H}_2\text{O}$  ( $\text{Na}_2\text{EDTA}$ ); Potassium dichromate ( $\text{K}_2\text{Cr}_2\text{O}_7$ ); Ascorbic Acid  $\text{C}_6\text{H}_8\text{O}_6$  (AA) and Rhodamine B (RhB) Diethylammonium chloride ( $\text{C}_{28}\text{H}_{31}\text{ClN}_2\text{O}_3$ ) were obtained from Sigma-Aldrich company and used without any purification.

Samples prepared by solvothermal process STP. Solution A was prepared by dissolving  $\text{Bi}(\text{NO}_3)_3 \cdot 5\text{H}_2\text{O}$  (5 mmol, 2.4253 g) in EG (10 mL) using ultrasound apparatus at room temperature until dissolved. Solution B was prepared by mixing GW (50–250 mg) in EG (10 mL) under ultra-sonication for 15 min at room temperature. Solution C contains PVP (100–300 mg) dissolved in EG (10 mL). To this solution 5 mmol of KBr and KI with respect to different molar ratio of  $\text{Br}/(\text{I} + \text{Br})$  (from 0 to 1) was added. First, solution B was added drop wise to solution A, and then, solution C was added drop by drop under moderate stirring for 30 min at room temperature. 80 mL of the obtained mixture was transferred to a 100 mL Teflon-lined stainless steel autoclave then heated under autogenous pressure in an oven at  $160^\circ\text{C}$  for 24 h. Afterward, the reactor was left to cool down by contact with air at room temperature; the product was collected by filtration, washed thoroughly with deionized water and ethanol then dried at  $80^\circ\text{C}$  for 12 h. Scheme 1 in the form of a flowchart summarizes the general approach to the preparation of materials by the two synthesis routes

For samples prepared by hydrothermal process HTP, all the preparations, concentrations and manipulation are the same than the



Scheme 1. Diagram 1 illustrates the general approach to materials preparation by the two synthesis routes.

STP, only EG was replaced by H<sub>2</sub>O. Table 1 summarizes the synthesis procedure by the two routes by assigning names to the obtained materials.

## 2.2. Characterizations

The photocatalyst materials in powder form were analyzed by XRD with a monochromatic Cu K $\alpha$ 1 radiation ( $\lambda = 1.54056 \text{ \AA}$ ) using an Empyrean PANalytical diffractometer. The morphology of the prepared photocatalysts was observed using a scanning electron microscope (SEM) HITACHI S-4800. N<sub>2</sub> adsorption-desorption isotherms at 77 K was carried out using a Tristar 3000 (Micromeritics, USA). The samples were first degassed under vacuum overnight at 100 °C. The specific surface area (SSa) values were determined by the BET method based on the adsorption isotherm. The size and volume of the pores were calculated using the BJH method on the isothermal desorption branch. The diffuse reflectance spectra (DRS) of the powder samples were analyzed in the 200–1000 nm range by a UV–visible spectrophotometer (JASCO V650) equipped with an integration sphere (JASCO ISV 922) using BaSO<sub>4</sub> as the internal reflectance standard. X-ray photoelectron spectroscopy (XPS) data were recorded using an ESCALAB 250 Thermoelectron spectrometer with a monochromatic source of Al K $\alpha$  radiation (1486.6 eV).

## 2.3. Adsorption study in dark

In order to evaluate the adsorption capacities of the prepared photocatalysts, adsorption kinetics were carried out in an open 500 mL beaker placed in a dark room. The experiment was carried out only with S-PVP-GW and S-PVP while respecting a solid/solution ratio of 1 g L<sup>-1</sup> and an initial dye concentration of 40 mg L<sup>-1</sup> at natural pH 4.4. The adsorption was evaluated by monitoring the residual concentration by UV–visible spectroscopy at 553 nm using a JASCO V-730 spectrophotometer.

## 2.4. Assessment of photocatalytic activity

Dyes photo-degradation was performed in an open beaker of 500 mL with 100 mg of photocatalyst dispersed in 100 mL of magnetically stirred aqueous solution of RhB (20–50 mg/L) at pH 4.4 resulting from the dissolution of the dye. The open beaker was placed under the lamp in a bath cooled with circulating water to keep the ambient temperature stable. After a 30 min in the dark to achieve the adsorption-desorption equilibrium, the stirred mixture was exposed to visible light provided by a 500 W tungsten lamp (TUNGSRAM trademark) emitting more than 400 nm and it was used without a cut-off filter. The

**Table 1**

Name, synthesis route with and without glass wool (GW), with and without PVP of the obtained materials (H for hydrothermal, S for solvothermal and M for mechanosynthesis) prepared with respect to the following molar ratios of BiOBr/BiOI (3:1).

Material named	Synthesis method	GW	PVP
H-PVP-GW	Hydrothermal	With	With
H-PVP	Hydrothermal	Without	With
S-PC	Solvothermal	Without	Without
S-GW	Solvothermal	With	Without
S-PVP	Solvothermal	Without	With
S-PVP-GW	Solvothermal	With	With
S-BiOBr-PVP-GW	Solvothermal	With	With
S-BiOI-PVP-GW	Solvothermal	With	With
S-BiOBr	Solvothermal	Without	Without
S-BiOI	Solvothermal	Without	Without
Bi <sub>2</sub> O <sub>3</sub> -PVP	Solvothermal	Without	With
M-PVP-GW	Mechanosynthesis	With	With

specifics of the lamp were properly presented in our previous works [22,40]. The maximum intensity of irradiance measured was 114.8  $\mu\text{W}/\text{cm}^2$  at 659.9 nm. The distance between the lamp and the surface of the solution in the beaker was kept fixed equal to 14 cm. Aliquot were collected at intervals time of 2 min, centrifuged and the dye concentration was determined as above. The calibration curve was established on RhB solutions in a concentration range of 0–20 mg L<sup>-1</sup> at natural pH 4.4. Neither oxygenation nor aeration was gassed in the solution. In addition, the initial pH was measured at first and not adjusted during the study.

## 2.5. Active species identification

Identification of the radical species responsible for photocatalytic efficiency was carried out in the presence of a few reagents known as radical species inhibitors such as ethanol (2 mmol L<sup>-1</sup>) as a scavenger of hydroxyl radicals, ascorbic acid (2 mmol L<sup>-1</sup>) as a scavenger of superoxide radicals anionic, (Na<sub>2</sub>EDTA, 1 mmol L<sup>-1</sup>) as hole scavenger and K<sub>2</sub>Cr<sub>2</sub>O<sub>7</sub> (1 mmol L<sup>-1</sup>) as electron traps [22,40–49].

## 2.6. Reusability study

The longevity and the stability of the best photocatalyst were studied for an initial RhB concentration of 20 mg L<sup>-1</sup> at natural pH 4.4 with a solid/solution ratio of 1 g L<sup>-1</sup>. After magnetic stirring in the dark for 30 min, the mixture was then exposed to visible light until total discoloration after 20 min, the photocatalyst was separated from the mixture by centrifugation and dried at 100 °C for 3 h, not ground and then added to a new RhB solution with a concentration identical to the first one in the same conditions than above. The stability of the photocatalyst was thus evaluated in the RhB degradation experiments repeated eight times.

## 3. Results and discussions

### 3.1. Synthesis and selections of the materials

The addition of GW and/or PVP in HTP or STP synthesis represents a novelty, therefore we hypothesized that, beside the Br/I molar ratio mentioned in the introduction, other parameters can affect the synthesis of the material as the time and temperature of reaction and, obviously the weight percentage of PVP and that of GW. These parameters have been studied in a set of preliminary tests (Supplementary Information) in order to determine the value of each parameter leading to the optimal photocatalytic activity of the material when briefly tested in RhB photo-discoloration (see tables presenting the screening of the parameters in Supplementary Information). This screening has shown that materials prepared by STP are generally better than those prepared by HTP. Moreover, the photocatalytic performances also appear linked to the weight percent of GW and PVP introduced during the synthesis, an optimum was observed for each of these two concentrations. Because it was not possible to characterize all the photocatalyst, we only report here the data of materials presenting the highest activity: those prepared with a molar ratio Br/I = 3 and with 5 w% of PVP and 3 w% of GW and with a especial attention to those prepared by STP that leads to the highest activity. The following labels are used: S and H for material prepared by STP and HTP respectively, GW if glass-wool was added, and/or PVP if the latter was added. Characterizations of other materials were undertaken only for comparison in view of a better understanding of the origin of the photocatalytic activity of the materials prepared by STP.

These photocatalysts were selected because of their high kinetic parameter value *k* (Fig. 1) compared to the other photocatalysts tested. The comparative study of the photodegradation kinetics between the two photocatalysts prepared by STP followed by the mechanistic

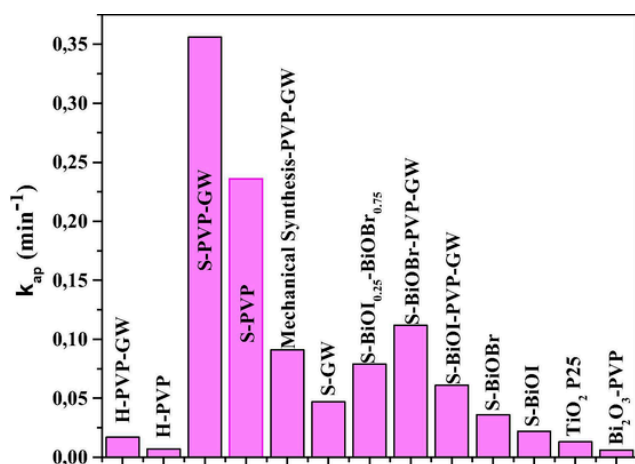


Fig. 1. Comparative study between prepared and benchmark Photocatalysts on RhB photocatalytic discoloration at 20 mg L<sup>-1</sup> under visible light.

study of photodegradation will be presented below after the structural characterization results. The  $k$  values were determined in standardized conditions (30 min of equilibration in the dark,  $T = 22 \pm 2$  °C, photocatalyst concentration of 1 g L<sup>-1</sup>, [RhB] = 20 mg L<sup>-1</sup> and pH = 4.4; the stirred mixture was exposed to visible light provided by a 500 W tungsten lamp (TUNGSRAM trademark) emitting more than 400 nm and it was used without a cut-off filter), the highest activity of the STP materials is obvious when compared to those prepared by HTP, moreover, it is much better than that of the bench mark P25 or Bi<sub>2</sub>O<sub>3</sub> or BiOI or BiOBr or Bi<sub>2</sub>O<sub>3</sub>-ZnO deposited on GW that we recently report [22]. Thus on the basis of the comparative results obtained relating to the kinetic constants between the various materials, we opted to carry out the photocatalytic study including adsorption for the two best materials synthesized by the solvothermal method.

In comparison with the results published in the literature, even at low initial concentrations of RhB (Table 2), S-PVP and S-PVP-GW present values of kinetic constants  $k$  two to three times higher than others materials reported concerning the photo-discoloration of RhB. The most relevant point of these data is that the presence of PVP or GW in the process leads to improve the activity of the materials in all the cases. Even more, the simultaneous presence of both, PVP and GW, causes crystal and surfaces structural modifications, thus leading to the highest improvement in photocatalytic activity.

### 3.2. Characterization of the prepared materials

#### 3.2.1. PXRD analysis

The normalized diffractograms patterns of the HTP (Fig. 2A) and STP (Fig. 2B) photocatalysts indicate the presence of several crystalline phases for these materials prepared in mild conditions (160 °C/24 h). The first observation made from XRD is that the addition of GW did not significantly modify either the crystallinity or the intensity of the peaks in the case of materials prepared by HTP. Differently, the presence of PVP always slightly broaden the signals of materials prepared by solvothermal process possibly due to smaller particles size as suggested by the observations reported by Shi et al.[34], Wang et al. [50] and Mahmmodi et al. [51].

Between the two solvothermal and hydrothermal methods, PVP has an effect on the crystal structure of materials prepared by STP. In fact, the PVP acts as an agent directing the structure along the direction of the plane (1 1 0) in comparison with the material prepared by STP without PVP. Indeed, the peak of the plane (1 0 2) on the diffractogram of BiOBr (JCPDS 73-2061) alone (prepared without PVP) appears with the same intensity as that of (1 1 0). On the other hand, when the PVP is added in the synthesis of the ternary composite, the most intense peak is that of the plane (1 1 0) of BiOBr (Fig. 2), a similar observation was reported by Yang et al. [52]. In addition, the presence of GW in the form of fiber acted as a surface allowing the deposit in the form of aggregates of crystals on the fiber surface offering to the semiconductor prepared by STP a specific surface extended compared to that without GW. However, for materials prepared by HTP, PVP did not have an effect as an agent directing the structure. Indeed, the most intense peak is that of the plane (0 0 1), whether for materials prepared with or without PVP. The third general observation is the absence of peaks of the BiOI phase on the diffractogram of the H-PVP-GW and H-PVP materials, suggests that the hydrothermal method could not have formed the two semiconductors together, probably due to the solubility of iodide in an aqueous medium compared to that of bromide.

Nevertheless, other low intensity peaks attributed to the  $\alpha$ -Bi<sub>2</sub>O<sub>3</sub> phase in good agreement with the database (JCPDS 41-1449) were observed in materials prepared only by STP. After a large reading of the literature, this being for the first time that the presence of the Bi<sub>2</sub>O<sub>3</sub> is observed in the synthesis of BiOX by the solvothermal route. Finally, no displacement of the peaks was observed on the diffractogram of the S-PVP-GW and S-PVP materials in comparison with those of BiOBr and BiOI separately, which may suggest that there is a mixture of three phases rather than a solid solution of the oxide of bismuth with the two oxy halides of bismuth.

Table 2

Comparative results of RhB photo-discoloration by different photocatalysts from the literature.

Photocatalysts	S <sub>BET</sub> (m <sup>2</sup> /g)	[RhB] (mg/L)	Photocatalyst Dosage (g/L)	Discolor (%)	Time (min)	Synthesis route	Ref
S-PVP-GW	65.45	20	1	100	18	Solvothermal (PVP/GW)	This work
S-PVP	48.08	20	1	100	20	Solvothermal (PVP)	This work
BiOBr/BiOI/Cellulose	116.5	25	0.4	100	30	Precipitation at 80 °C	[30]
BiOBr/BiOI (80%/20%)	-	14.4	1	90	60	Solvothermal	[11]
BiOBr/BiOI (50%/50%)	24.44	15	0.4	100	40	Solvothermal (PVP)	[39]
BiOBr <sub>1-x</sub> I <sub>x</sub> (x = 0.8)	10.8	20	0.33	99	90	Hydrothermal	[40]
15% Br-BiOI	8.62	14.4	1	100	150	Precipitation at 80 °C	[41]
$\alpha/\beta$ Bi <sub>2</sub> O <sub>3</sub>	-	4.8	1	92.6	210	Solvothermal	[42]
BiOBr/BiOF	-	10	1	100	25	Hydrothermal	[43]
ZnO/BiOBr/BiOI (20%)	32.1	4.8	0.4	100	90	Precipitation under reflux	[44]
Fe <sub>3</sub> O <sub>4</sub> /BiOBr/BiOI	48.30	20	0.35	99.2	80	Solvothermal	[45]

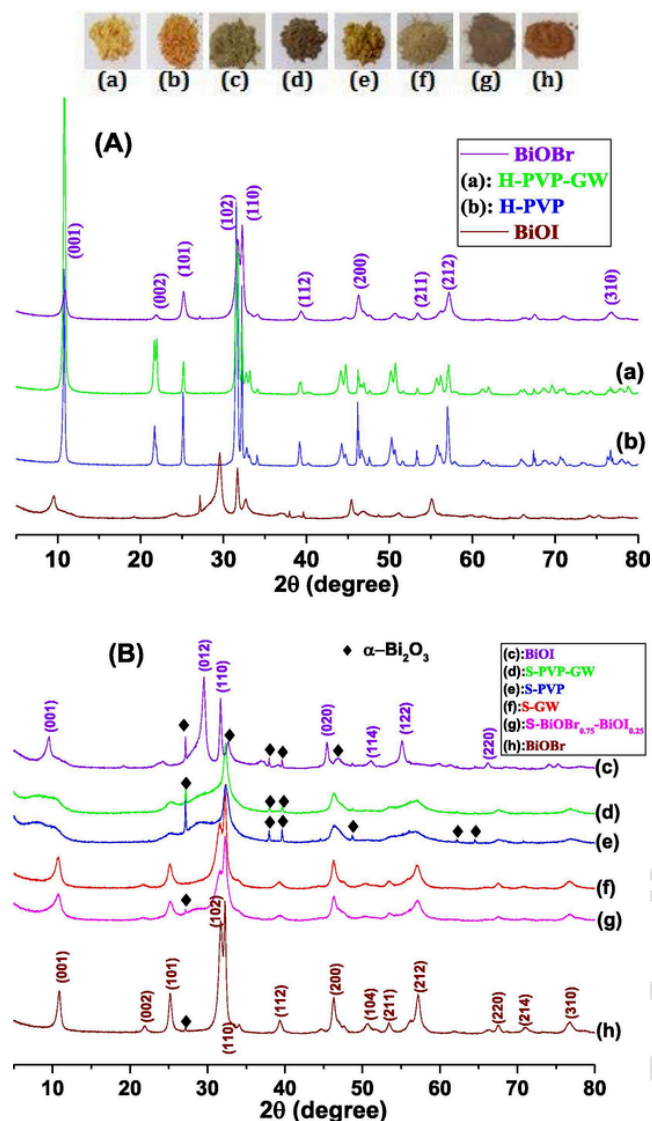


Fig. 2. X-ray diffraction patterns of photocatalysts prepared by STP and HTP and reference materials BiOI and BiOBr.

### 3.2.2. XPS analysis

The surface elementary states and the chemical composition examined by X-ray photoelectron spectroscopy (XPS) were possible only on a limited number of samples: H-PVP; H-PVP-GW; S-PVP and S-PVP-GW. The main difference between the survey spectrums (Fig. 3) of the different photocatalysts is the intensity of the peaks of the iodine element more intense for STP materials compared to the HTP ones, despite the same initial amounts of iodide reagents in both preparations. The I 3d spectrum of the materials prepared by HTP shows two signals with low intensities having binding energies located at 629.9 for I 3d<sub>3/2</sub> and 618.4 eV for I 3d<sub>5/2</sub>, in the literature, these binding energy values correspond to I<sup>-</sup> ions [31,53–55]. Besides, the signals' intensity is higher for material without GW (H-PVP) compared to those with GW, namely H-PVP-GW. These results show the presence of iodide in small quantities within the PCs prepared by the HTP as shown in the Table 3 relating to the chemical composition determined by XPS in comparison with that found by EDX. For S-PVP-GW and S-PVP prepared by STP, the higher signal intensity is observed for the binding energy peaks of I 3d of iodide species, 618.8 for I 3d<sub>5/2</sub> and 630.4 for I 3d<sub>3/2</sub>. STP and HTP materials also differ by the Bi 4f contribution, while H-PVP-GW and H-

PVP exhibits binding energy respectively for Bi 4f<sub>5/2</sub> (164.60 and 159.26 eV) and Bi 4f<sub>7/2</sub> (164.29 and 158.96 eV) in agreement with an oxidation state +3 [34,56–59]. Differently, the Bi 4f XPS spectra of STP materials show 4 peaks after the deconvolution. It is possible to identify binding energy for Bi 4f<sub>5/2</sub> at 164.12; 165.33 eV in S-PVP and 164.16; 165.41 eV in S-PVP-GW and for Bi 4f<sub>7/2</sub> at 158.81; 160.26 eV in S-PVP and 158.85; 160.35 eV in S-PVP-GW. At present, these additional peaks in the spectra STP materials are ascribed to the presence of α-Bi<sub>2</sub>O<sub>3</sub> phase in agreement with the XRD data which showed the absence of the Bi<sub>2</sub>O<sub>3</sub> phase in the materials prepared by hydrothermal. The presence of glass wool didn't visibly change the oxidation state of bismuth in the photocatalyst prepared by either HTP or STP.

For the Bromine, the Br 3d spectrum exhibits two distinct peaks with values varying from 68.63 to 68.90 eV for Br 3d<sub>3/2</sub> and from 67.69 to 67.95 eV for Br 3d<sub>5/2</sub> for materials prepared by both synthetic routes. The O 1s spectra of the photocatalyst indicated a rather complex situation, the signal was fitted by deconvolution in three peaks from 529.50 to 532.85 eV assigned respectively to Bi—O, C—O and O—H bonds [22,40,54,55]. The results of elemental analysis by XPS and EDX (Table 3) show that S-PVP-GW has higher atomic rates of Bi, Br and I than S-PVP. This can result in an abundance of the three oxides Bi<sub>2</sub>O<sub>3</sub>, BiOBr and BiOI in S-PVP-GW than in S-PVP. This will likely have an effect on better photocatalytic efficiency for S-PVP-GW than S-PVP.

### 3.2.3. SEM analysis

Fig. 4 shows the morphology of the PCs observed by SEM. The images at different magnifications of the sample prepared by HTP in the presence of GW (H-PVP-GW) show apparently unmodified glass fibers with few fragments of petals probably those of the composite BiOI/Br. Clearly, the photocatalyst is not mostly deposited or supported on the glass fiber surface. It is mostly present as individual non-regular octagonal petals as well as desert sand micro-roses made of these petals. The same observations are also made on the other HTP material without GW (image of H-PVP). Differently, for STP materials, the images at different magnifications show different shapes in the presence of GW (image of S-PVP-GW) than those of PCs prepared by hydrothermal. In addition, here the GW fibers are well covered by micro-spheres in the form of cauliflower-like agglomerated together formed by petals of smaller sizes than those observed on images of PCs synthesized hydrothermally. The same shape was observed from the images of material prepared by STP without GW (image of S-PVP) but with a size slightly larger than that of S-PVP-GW.

### 3.2.4. N<sub>2</sub> adsorption-desorption analysis

The N<sub>2</sub> adsorption-desorption isotherm at 77 K are very similar for all the samples, showing a type IV pattern with hysteresis loops of type H3 (Fig. S1). A slight difference exists between hydrothermal and solvothermal processed materials, the hysteresis loops is weaker in the case of materials prepared by HTP probably indicating a macroporosity of the two materials. Unlike the materials synthesized by the solvothermal route, the hysteresis loop is more open, probably due to the mesopore characters of the two materials. From these results, the BET specific surfaces area then the total pore volume measured at P/P<sub>0</sub> = 0.99 and pore size determined according to BJH method from desorption isotherm branch are presented in Table 4. As a general observation, the materials synthesized by STP have higher specific surfaces than those prepared by HTP. The PC prepared by solvothermal in the presence of PVP without GW (S-PVP) displays a specific surface area of 48.1 m<sup>2</sup> g<sup>-1</sup>. The addition of GW has a rather high effect, increasing the surface area up to 65.5 m<sup>2</sup> g<sup>-1</sup> (S-PVP-GW). In contrast, the average pore diameter and pore volume of S-PVP are much greater than that of S-PVP-GW. Thus, for the materials prepared by the solvothermal process, the addition of GW caused an improvement of ≈35% in spe-

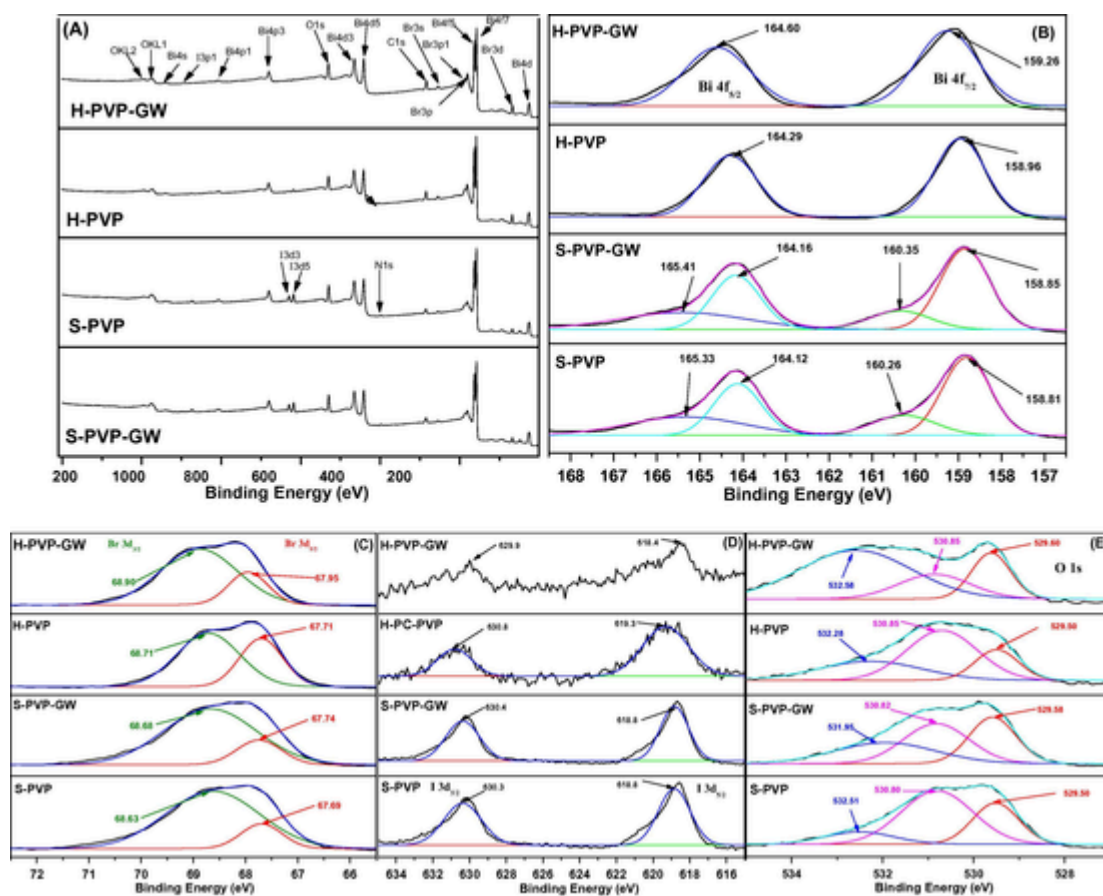


Fig. 3. XPS analysis of photocatalysts prepared by HTP and STP with PVP and with or without GW: (A) survey, (B) Bi 4f, (C) Br 3d, (D) I 3d and (E) O 1s respectively.

Table 3

Elementary composition from XPS and EDX analysis of prepared materials.

Photocatalysts	% Atomic from XPS					% Atomic from EDX				
	Bi	O	I	Br	C	Bi	O	I	Br	C
S-PVP-GW	16.08	37.63	2.40	8.47	35.42	11.11	24.24	0.78	5.11	53.15
S-PVP	17.82	40.05	2.24	8.08	31.80	7.86	20.24	0.63	2.76	68.52
H-PVP-GW	12.82	34.17	0.12	11.24	41.65	11.19	30.40	0.53	13.41	40.57
H-PVP	14.47	29.25	0.36	12.77	43.47	4.99	13.97	0.22	6.44	74.39

cific surface area compared to the material without the glass wool. The same remark was made by Benyamina et al. when using GW in the synthesis of  $\text{Bi}_2\text{O}_3\text{-ZnO}$  photocatalyst [22].

### 3.2.5. UV-Vis diffuse reflectance spectroscopy

This technique was used to determine the optical properties and the band gap energy of the synthesized materials. The results in the form of reflectance (R %) are presented in Fig. 5(a). The values of the band gap energies ( $E_g$ ) of the prepared photocatalysts were determined from the data plotting (Fig. 5(b)) according to the modified Kubelka-Munk equation described below.

$$(F(R)h\nu)^{1/n} = \beta(h\nu - E_g) \quad (1)$$

$$F(R) = \frac{(1-R)^2}{2R} \quad (2)$$

In the graphical presentation, the modified function of Kubelka-Munk is similar to that of the Tauc plot, and has been used in the literature by several authors [60–63].

Where  $F(R)$ ,  $h$ ,  $\nu$ ,  $\beta$  and  $E_g$  are Kubelka-Munk function, the Planck's constant (J.s), the light frequency ( $\text{s}^{-1}$ ), the proportionality coefficient and the band gap energy (eV) respectively. The constant  $n$  depends on the electronic transition type between the two valence and conduction bands and its value can be 1/2 or 2 for a direct or indirect transition respectively. Based on previous work by different authors, it has been concluded that the electronic transition is indirect for  $\text{BiOI}$ ,  $\text{BiOBr}$  and  $\text{Bi}_2\text{O}_3$  [10,64–66]. Thus the plotting of the modified K-M function  $(F(R)h\nu)^{1/2}$  versus  $h\nu$  allowed the determination of the band gap energy of the material by extrapolation of the linear part of each curve with the x-axis and band gap energy values are presented in Table 4. It appears that the lowest band gap energy values (2.00 and 2.21 eV) are obtained with the materials prepared by the HTP. Besides, the pres-

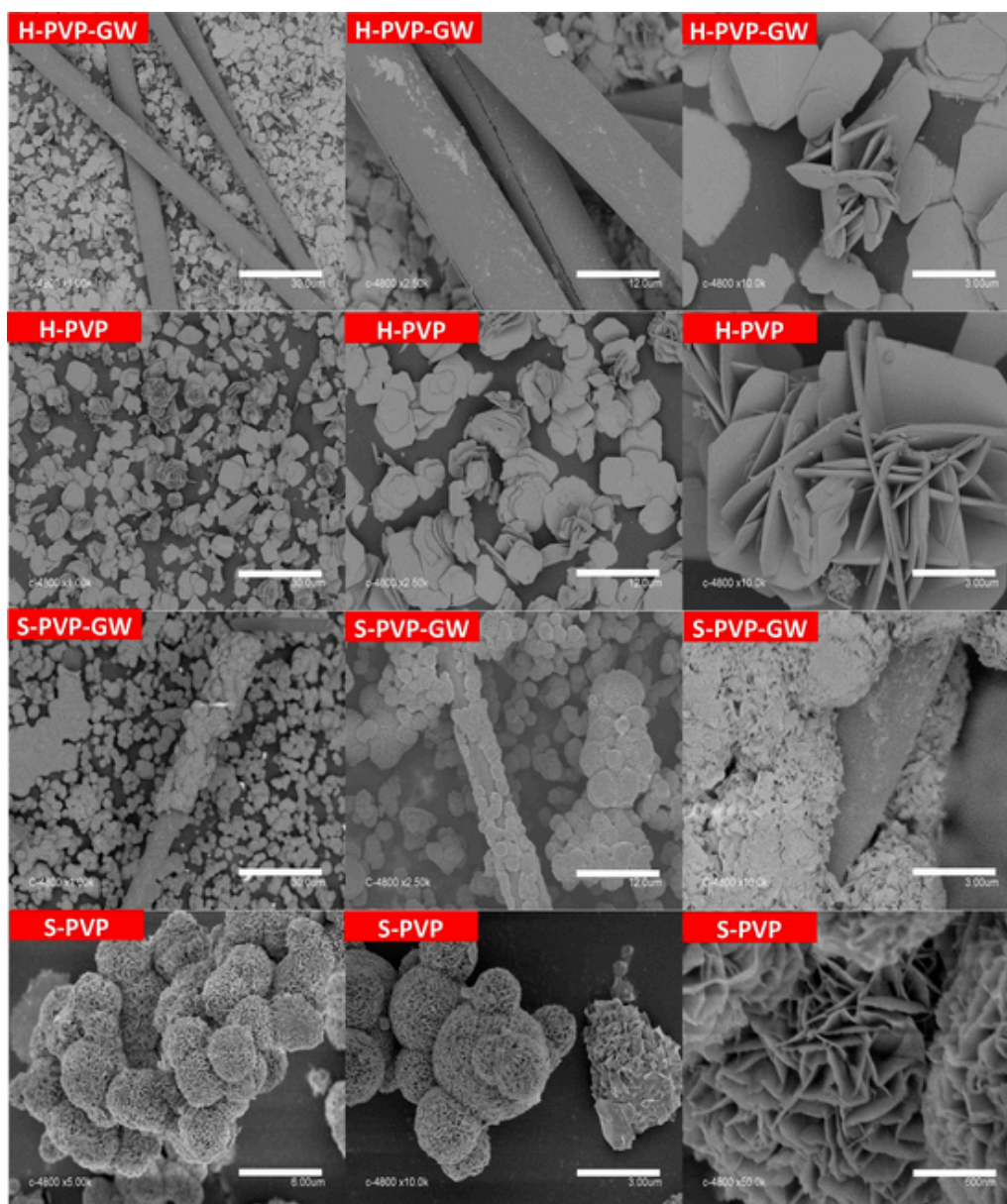


Fig. 4. SEM images at different magnifications of H-PVP-GW, H-PVP, S-PVP-GW and of S-PVP composites.

Table 4

Textural and optical properties of prepared composites obtained from adsorption-desorption of  $N_2$  at 77 K and UV-vis DRS.

Photocatalysts	$S_{BET}$ ( $m^2/g$ )	$S_{Ext}$ ( $m^2/g$ )	D (nm)	V ( $cm^3/g$ )	$E_g$ (eV)
H-PVP-GW	5.06	4.84	7.66	0.004	2.21
H-PVP	2.45	2.10	12.71	0.009	2.00
S-PVP-GW	63.45	59.78	8.30	0.023	2.43
S-PVP	48.08	47.54	16.07	0.177	2.23

ence of GW during the processing lead to an increase of the band gap energy for materials prepared by both routes (2.21 and 2.23 eV).

### 3.3. Photocatalytic activity study

#### 3.3.1. Adsorption in dark

Fig. 6 shows firstly that the adsorption kinetics of RhB is rapid ( $< 10$  min) and stabilizes after 20 min, secondly a better adsorption capacity is measured with the materials prepared without GW (S-PVP) despite its small specific surface area compared to the material prepared with GW (S-PVP-GW). This may be due to the average pore size of S-PVP (16.07 nm) and to pore volume (0.177  $cm^3/g$ ) which are much greater than that of S-PVP-GW (8.30 nm and 0.023  $cm^3/g$ ). All the kinetic studies disclosed below include an equilibration time of 30 min.

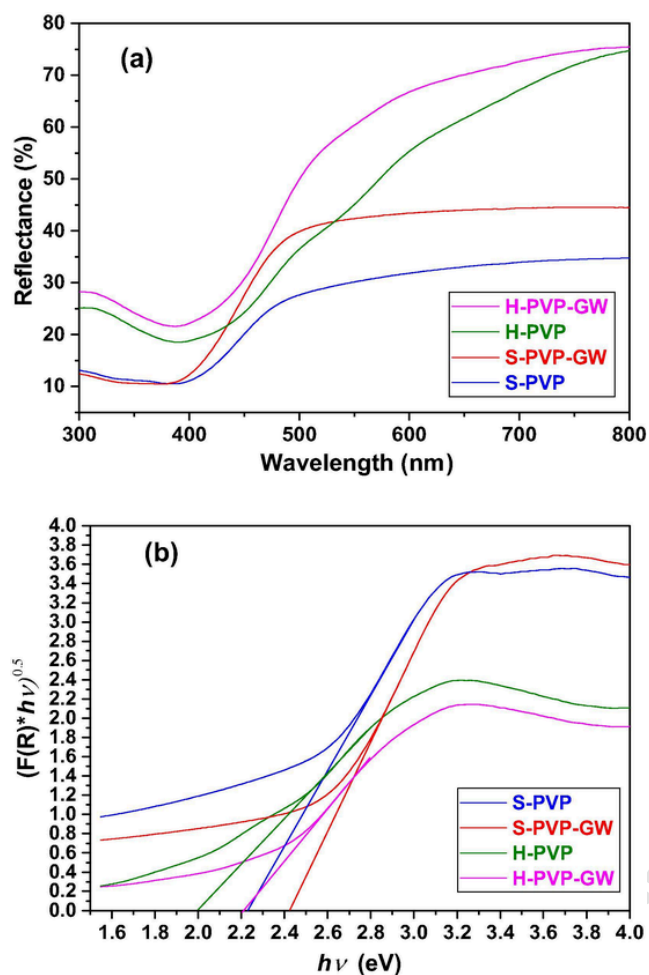


Fig. 5. The Kubelka-Munk function plots versus wavelength from UV–visible DRS (a) and modified Kubelka-Munk function plots versus  $h\nu$  (b).

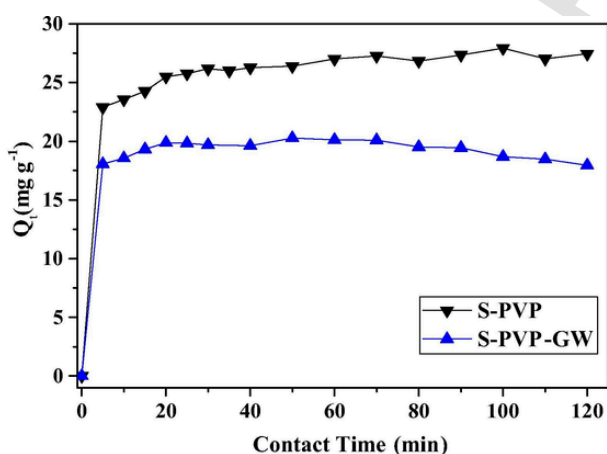


Fig. 6. Sorption kinetics of RhB on S-PVP and S-PVP-GW ( $C_i = 40 \text{ mg L}^{-1}$ ,  $\text{pH}_i = 4.44$  and  $1 \text{ g L}^{-1}$  of solid/solution ratio).

### 3.3.2. Kinetics study of photo-discoloration

The kinetic study of the photo-discoloration of RhB at different initial concentration was carried out with the materials S-PVP and S-PVP-GW to highlight the effect of the presence of GW on the photocatalytic efficiency under visible light. Thus, the plots of the ratio  $C_{i,\text{corr}}/C_t$  of the dye photo-discoloration versus time are presented in Fig. 7(a) and

(b). A blank test performed with only a powder of GW as demonstrate the absence of photo-discoloration of a solution of RhB. The best result in terms of photo-discoloration kinetics is obtained with the material prepared with GW and PVP, namely S-PVP-GW probably attributed to its high specific surface area compared to that of material prepared without GW (S-PVP) despite having a lower adsorption capacity towards RhB than that of S-PVP. This can be explained by the fact that part of the surface of S-PVP-GW is unoccupied by RhB molecules but probably occupied by both  $\text{O}_2$  and  $\text{H}_2\text{O}$  which presumably contribute in the formation of radical species causing a probably different degradation mechanism that of S-PVP. This is probably owing to the morphology and the small size of the microspheres of the composite arranged on the GW fibers (S-PVP-GW) compared to that of composite without GW (S-PVP) which could allow reflections of light thanks to its narrow band gap, thus leading to better collection of photons by the different surfaces of the microspheres, which would probably increase the separation of the photo-generated charges ( $e^-/h^+$ ). The latter will thus be more available in participation in reactions with adsorbed species (RhB;  $\text{O}_2$ ,  $\text{H}_2\text{O}$ ; among others). This is probably due also to the difference in quantity of the three atoms forming the three phases of the composite between S-PVP and S-PVP-GW. Indeed, it appears from the results of XPS and EDX (Table 3) that the atomic percentages of Bi, Br and I are higher in S-PVP-GW than those of S-PVP. This means that the three oxides ( $\text{Bi}_2\text{O}_3$ ,  $\text{BiOBr}$  and  $\text{BiOI}$ ) are more abundant in S-PVP-GW than in S-PVP. The latter can therefore be positioned in lower photocatalytic efficiency than S-PVP-GW. Indeed, a total discoloration of RhB at  $20 \text{ mg L}^{-1}$  was achieved after only 18 min with S-PVP-GW against 20 min with S-PVP. To best of our knowledge, these results are among the best ones in the literature [46–49,67] (see Table 2). Fig. 7(c) and (d) shows the spectral evolution of RhB solution at  $20 \text{ mg L}^{-1}$  as a function of the photo-degradation time until total discoloration in the presence of S-PVP and S-PVP-GW respectively. The absorption peak corresponding to  $\lambda_{\text{max}}$  of 553 nm decreases gradually and shifted to 495 nm (blue-shift) and then disappears with photodegradation time; there is a hypsochromic shift of approximately 58 nm. According to the literature, this blue-shift is due to the loss of the N-ethyl group of the RhB molecule (an N de-ethylation) caused probably by the attack of the two radical species, the hole ( $h^+$ ) and the superoxide anion ( $\text{O}_2^-$ ) photo-generated by the materials S-PVP-GW and S-PVP. Even more, alone with S-PVP-GW, this attack is accelerated by the hydroxyl radical ( $\text{HO}^\bullet$ ) by targeting the central carbon atom as reported by literature [68–70], thus resulting in the disappearance of the chromophore of RhB, probably forming the carboxylic acids (by-products).

In order to evaluate the kinetics of the photo-discoloration of RhB by the prepared photocatalysts S-PVP and S-PVP-GW, the pseudo-first order model presented by the equation below has been used.

$$\ln \left( \frac{C_{i,\text{corr}}}{C_t} \right) = k_{\text{app}} t \quad (3)$$

where  $C_{i,\text{corr}}$  (mg/L) is the corrected initial dye concentration (after adsorption in dark) and  $C_t$  (mg/L) is the concentration at time  $t$  (min) of the RhB dye,  $k_{\text{app}}$  ( $\text{min}^{-1}$ ) is the constant of apparent kinetics. The values of the latter (Table 5) were determined from the plots of  $\ln \left( \frac{C_{i,\text{corr}}}{C_t} \right)$  vs time  $t$  presented in Fig. 7(e) and (f) for S-PVP and S-PVP-GW respectively. The obtained kinetic results are consistent with the pseudo-first order model according to the correlation values  $R^2$  which greatly exceed 0.96.

The kinetics and the reaction mechanism in heterogeneous photocatalysis depend on several parameters, among them, the surface properties which influence on adsorption. The kinetic model which describes the reaction speed by associating the two constants of adsorption and kinetics and function of the concentration is that of Langmuir-Hinshlwood (L–H) presented by the following equation in the lin-

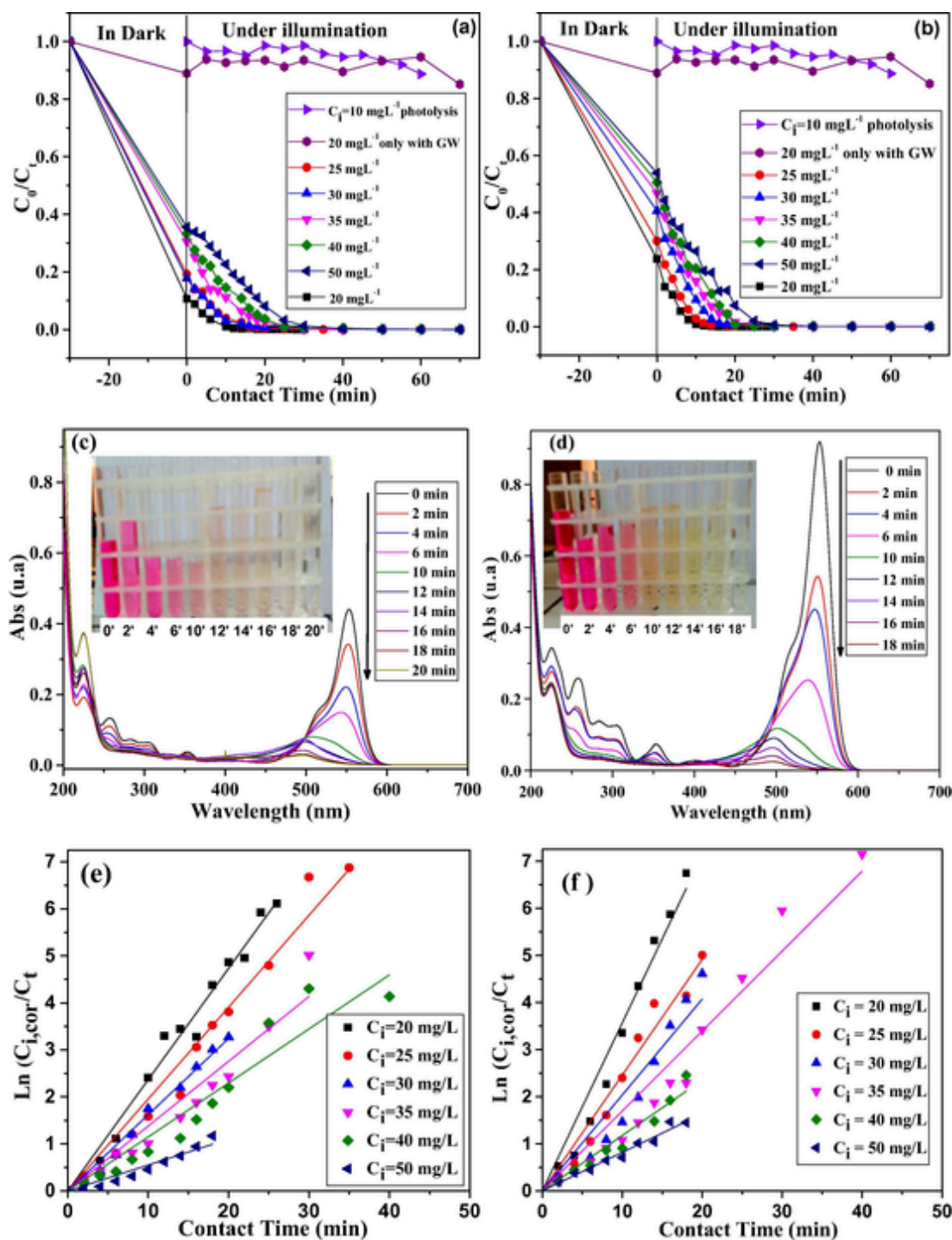


Fig. 7. (a and b) kinetics of photo-discoloration under visible light at different concentrations of RhB by S-PVP and S-PVP-GW respectively, (c and d) spectral evolution of RhB at 20 mg L<sup>-1</sup> after photo-degradation at different sampling times versus wavelength with S-PVP and S-PVP-GW respectively, (e and f) first-kinetic linear plots of RhB photocatalytic discoloration at various initial dye concentrations under visible light with S-PVP and S-PVP-GW respectively.

earized form [71,72].

$$\frac{1}{r_i} = \frac{1}{k_{L-H}} + \frac{1}{k_{L-H}K_{ads}} \frac{1}{C_{i,corr}} \quad (4)$$

The constants values (Table 5) were determined from the plot of 1/r<sub>i</sub> versus 1/C<sub>i,corr</sub> (Fig. 8).

Where, r<sub>i</sub> (mg L<sup>-1</sup> min<sup>-1</sup>) is the initial rate of the photocatalytic discoloration, C<sub>i,corr</sub> is the initial dye concentration corrected after adsorption in dark (mg/L), k<sub>L-H</sub> (mg L<sup>-1</sup> min<sup>-1</sup>) is the Langmuir-Hinshel-

wood rate constant, and K<sub>ads</sub> is the adsorption equilibrium constant on photocatalyst in (mg/L)<sup>-1</sup>.

It appears that from the K<sub>L-H</sub> values found 3.56 and 2.43 mg L<sup>-1</sup> min<sup>-1</sup> for S-PVP-GW and S-PVP respectively, that the kinetics of RhB photo-discoloration by S-PVP-GW is approximately 1.46 times faster than with S-PVP; thus indicating the advantageous role of GW in increasing the specific surface area by 1.36 times that of the material without GW and subsequently improving the kinetic performance

Table 5

Kinetics parameters of RhB photo-discoloration at different initial dye concentration with S-PVP and S-PVP-GW under visible light.

Photocatalyst	$C_i$ (mg/L)	$C_{i,cor}$ (mg/L)	$k_{app}$ (min <sup>-1</sup> )	$r_i$ (mg L <sup>-1</sup> min <sup>-1</sup> )	$R^2$
S-PVP-GW	20	4.45	0.3567	1.5897	0.9882
	25	7.37	0.2457	1.8109	0.9863
	30	12.13	0.2036	2.4692	0.9701
	35	16.2	0.1697	2.7488	0.9754
	40	20.22	0.1176	2.3783	0.9798
S-PVP	50	27.22	0.0817	2.2282	0.9921
	20	2.01	0.2367	0.4758	0.9945
	25	4.73	0.1955	0.9245	0.9882
	30	5.31	0.1621	0.8609	0.9956
	35	10.57	0.1379	1.4573	0.9727
40	13.31	0.1149	1.5289	0.9632	
50	18.05	0.0551	0.9952	0.9690	

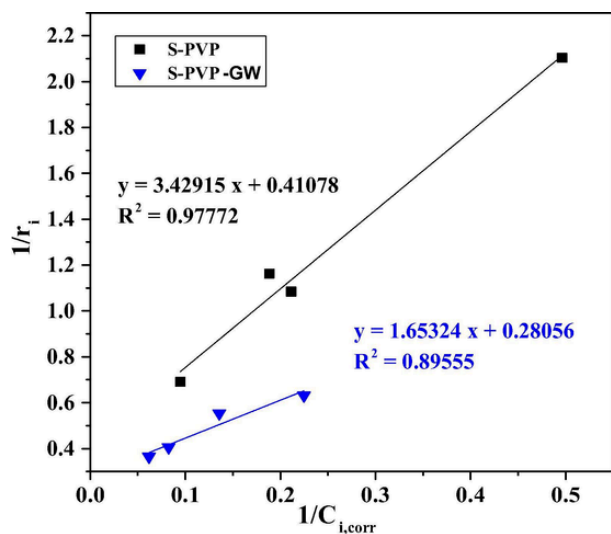


Fig. 8. Langmuir-Hinshelwood kinetic model plots of RhB photo-discoloration under visible light by S-PVP and S-PVP-GW ( $pH_i = 4.4$  and solid/solution ratio =  $1 \text{ g L}^{-1}$ ).

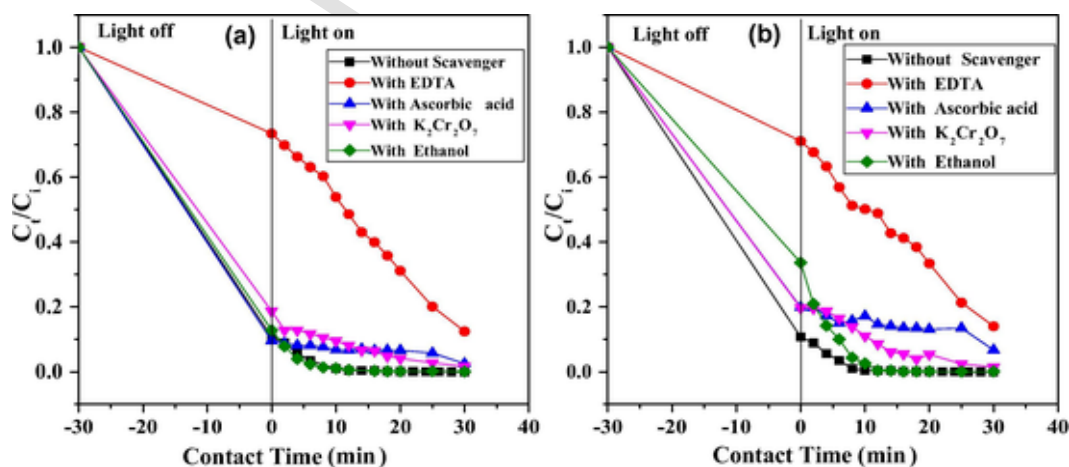


Fig. 9. Identification of active species responsible for the photo-discoloration of RhB under visible light by (a) S-PVP and (b) S-PVP-GW after the addition different scavengers with the respect to the following conditions:  $C_i = 20 \text{ mg L}^{-1}$ ;  $pH_i = 4.4$  and solid/solution ratio  $1 \text{ g L}^{-1}$ .

in the RhB photo-degradation with probably a more different reaction mechanism with S-PVP-GW than with S-PVP.

### 3.3.3. Active species identification

The photo-degradation of organic pollutant can be done by various radical species which contribute in an individual or mutual way. The identification of the contribution of each species (hydroxyl radical ( $\text{HO}^\bullet$ ), superoxide anion radical ( $\text{O}_2^{\bullet-}$ ) and photo-generated holes ( $h^+$ ) and electron ( $e^-$ )) is based on the inhibition of each species by the addition of a radical scavenger during photo-degradation [22,40–42,73]. The plot of  $C_t/C_i$  vs contact times in Fig. 9 shows the effect of each inhibitor on the photocatalytic efficiency of S-PVP (Fig. 9(a)) and S-PVP-GW (Fig. 9(b)) towards the RhB discoloration. Thus, a 100% of discoloration is observed without any scavengers after 20 and 18 min in presence of S-PVP and S-PVP-GW respectively. When EDTA (as  $h^+$  inhibitor) was added, the discoloration was only 80% after 20 for S-PVP and 61% after 18 min for S-PVP-GW respectively. Furthermore, not more than 94 and 86% of discoloration rates in the presence of S-PVP and S-PVP-GW respectively were achieved during the same irradiation time when ascorbic acid (as  $\text{O}_2^{\bullet-}$  scavenger) was used. A slight decrease in the discoloration percentage for both materials was observed when  $\text{K}_2\text{Cr}_2\text{O}_7$  (as an electron scavenger) was added. Finally, the addition of ethanol (as  $\text{HO}^\bullet$  scavenger) did not modify the percentage of photo-discoloration in the presence of S-PVP compared to the case without scavenger, but it is not the case for S-PVP-GW, there was a small reduction in discoloration when adding ethanol.

Altogether, the sum of these data shows an almost similar mechanism of photo-degradation of RhB between the two materials, although the overall efficiency of the process is higher for S-PVP-GW. The main reactive specie responsible for RhB photo-degradation has been identified as the hole ( $h^+$ ) with a moderate contribution of  $\text{O}_2^{\bullet-}$  for both materials. Even more, a third moderate contribution of  $\text{HO}^\bullet$  was also identified only with S-PVP-GW.

### 3.3.4. Proposal photocatalytic reaction mechanism

On the basis of the characterization results these materials contain three different semiconductors ( $\text{BiOBr}$ ,  $\text{BiOI}$  and  $\text{Bi}_2\text{O}_3$ ) in quite unequal proportions. Thus, a possible electronic transition scheme can be proposed in order to describe the reaction mechanism of the degradation of RhB. First, the positions of the edge of the valence (VB) and conduction (CB) bands were determined from the following equations [13,49,59]:

$$E_{\text{VB}} = E_g + E_{\text{CB}} \quad (5)$$

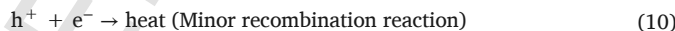
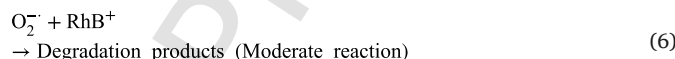
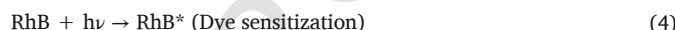
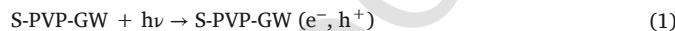
$$E_{CB} = X - E_C - 0.5E_g \quad (6)$$

where  $E_C$  is the energy of the free electrons on the hydrogen scale, which is approximately 4.5 eV and  $X$  represents the absolute electronegativity of each photocatalyst determined by the geometric mean of the electronegativity of each atom calculated according to Mulliken scale [74,75]. So the values of  $X$  are 6.35; 6.11 and 6.12 eV for BiOBr; BiOI and  $\text{Bi}_2\text{O}_3$  respectively which approximate those in the literature [13,76]. The  $E_{VB}$  and  $E_{CB}$  values determined from Eqs. (5) and (6) are 3.26 and 0.65 eV for BiOBr; 2.58 and 0.83 eV for BiOI and 3.04 and 0.2 eV for  $\text{Bi}_2\text{O}_3$  respectively and are very close to those found in literature [43,49,76,77]. Also important here, the values of LUMO and HOMO of RhB are  $-1.42$  and  $0.95$  eV respectively [49,67].

Photon of the visible light ( $>400$  nm) have energy  $<3.2$  eV therefore, higher to the band gap energy of each of the three semiconductors. The photo-excitation of electrons from the valence band (VB) to the conduction band (CB) of BiOBr,  $\text{Bi}_2\text{O}_3$  and/or BiOI of S-PVP and S-PVP-GW conducts to formation of pair  $e^-/h^+$  (reactions (1) and (2)). The photonic energy of the visible light ( $>400$  nm) corresponds to less than 3.2 eV can simulate the  $e^-$  of the VB of BiOI up to a less negative energy level of  $-0.62$  eV or another level of VB of  $\text{Bi}_2\text{O}_3$  ( $-0.16$  eV) than that of the couple  $\text{O}_2/\text{O}_2^-$  ( $-0.046$  eV NHE) [78,79]. In fact, at these two VB positions of  $\text{Bi}_2\text{O}_3$  or BiOI, the dissolved oxygen reacts to produce the superoxide anion radical ( $\text{O}_2^-$ ) (reaction (3)). Besides, the RhB dye has a maximum absorption in the visible at 553 nm (energy greater than or equal to 2.24 eV), thus allowing excitation of the electrons from HOMO to LUMO (dye sensitization) by giving excited RhB ( $\text{RhB}^*$ ) (reaction (4)), then the electron jumps from LUMO to CB of  $\text{Bi}_2\text{O}_3$  and/or CB of BiOI to give  $\text{RhB}^+$  (reaction (5)). The latter reacts with the  $\text{O}_2^-$  generating intermediate products (reaction (6)). A probable de-ethylation of RhB would be produced by reaction with the hole ( $h^+$ ) of the VB of the BiOI the closest (reaction (7)). Indeed, Hu et al. [80] reports that N de-ethylation is caused by direct attack of RhB through the hole ( $h^+$ ).

The relative position of all the energy levels is presented as diagram in Fig. 10, thus, charge transfer is created between the energy levels of the dye and those of the three semiconductors of the composite as well as the probable reactions of the RhB degradation mechanism.

From the active species identification, we learn that  $h^+$  is the main active one (reaction (7)). Besides,  $h^+$  is assumed to react also with the  $\text{H}_2\text{O}$  to form the hydroxyl radical ( $\text{HO}^\bullet$ ) (reaction (8)) because the potential of the couple  $\text{H}_2\text{O}/\text{HO}^\bullet$  of a value of 1.99 eV is lower than that of CBs of BiOBr,  $\text{Bi}_2\text{O}_3$  or BiOI. This radical contributes moderately in the RhB degradation only with S-PVP-GW (reaction (9)). It would also seem that the recombination of the electron-hole ( $e^-/h^+$ ) pair is very weak (reaction (10)). Thus, the mechanism of photo-degradation of RhB by the two photocatalysts is at present described by an association of following reactions:



### 3.3.5. Reusability study

All the photocatalysts present a high level of reusability, however, a slight reduction of  $\approx 8\%$  of the photocatalytic activity after 8 cycles is observed for S-PVP while the photo-discoloration yield is almost preserved ( $\approx 99\%$ ) for S-PVP-GW suggesting a higher stability in this case (Fig. 11(a) and (b)). This can be probably explained by the different mechanism of photo-degradation between S-PVP and S-PVP-GW. Indeed, for S-PVP-GW three radical species ( $h^+$ ,  $\text{O}_2^-$  and  $\text{HO}^\bullet$ ) con-

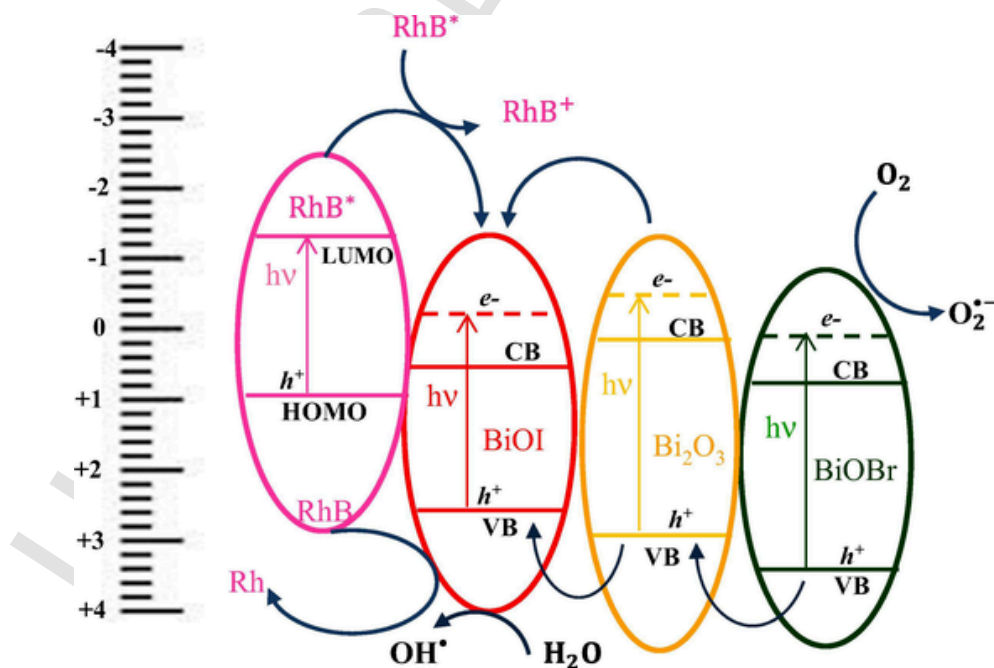


Fig. 10. Schematic illustration of the electronic transition between the different bands.

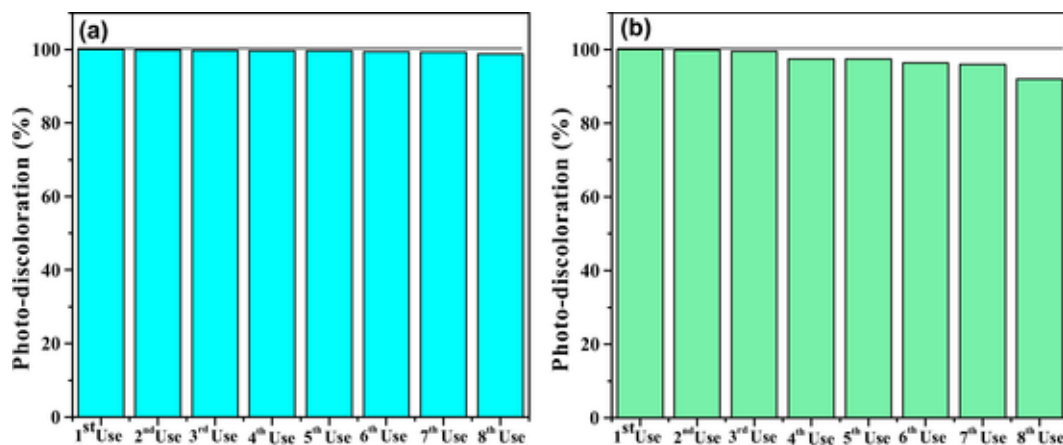


Fig. 11. Stability performance of (a) S-PVP-GW and (b) S-PVP after 8 use ( $C_i = 20 \text{ mg L}^{-1}$ ,  $\text{pH}_i = 4.44$  and solid/solution ratio =  $1 \text{ g L}^{-1}$ ).

tribute on the degradation of RhB against two species for S-PVP ( $h^+$ ,  $\text{O}_2^-$ ). This highlights the effect of the presence of glass wool as an inert support on the stability of the photocatalyst and making it as a candidate in the field of practical application on a real scale. The material S-PVP-GW was characterized again by XRD and it appears from Fig. S2 (in Supporting Information) that overall, there was no structural modification of the material S-PVP-GW after use in comparison with the same material before use; which indicates that the main structure of the S-PVP-GW composite was not destroyed and was sufficiently stable during 8 cycles of use.

#### 4. Conclusion

The present study is a contribution to identify new avenues for improving the efficiency of already known photoactive materials. Here is disclosed for the first time an unexpected combined effect between glass wool and PVP on the preparation giving access to a ternary composite  $\alpha\text{-Bi}_2\text{O}_3\text{-BiOI-BiOBr}$  having crystalline and surface properties leading to photocatalytic activity under visible light better than those of the other tested. The data confirmed an already reported observation, saying that photocatalysts prepared by solvothermal process exhibit a higher photocatalytic activity under visible light than that those prepared by hydrothermal process. But more importantly PVP combined with glass wool during the synthesis of the photocatalyst have a positive effect in improving the photocatalytic activity and the stability of the material. Moreover, the materials present different photo-degradation mechanism depending on the presence of glass wool and/or PVP, a possible explanation the efficiency improvement; meanwhile these data open discussion on their role in structuring the material. Indeed, the morphology and the small size of the microspheres of the composite arranged on the fibers of GW (S-PVP-GW) compared to that of composite without GW (S-PVP) could allow reflections of light thanks to the low band gap; thus improving the collection of photons which would probably increase the quantity of photo-generated electrons-holes which will be available in the participation in the reactions with adsorbed species as RhB,  $\text{O}_2$ ,  $\text{H}_2\text{O}$ , and others. The presence of three semiconductors together more abundant in S-PVP-GW than in S-PVP probably had an effect on the photocatalytic efficiency of S-PVP-GW compared to S-PVP. Further optimization of this new approach can lead to good candidates in real practical applications in the degradation of water-soluble organic pollutants or present in air, and probably as antibacterial layer.

#### CRediT authorship contribution statement

**Meriem Mansour:** Investigation, Methodology. **Imane Benyamina:** . **Bahia Benalioua:** Methodology, Validation. **Abdelhadi Bentouami:**

Project administration, Methodology, Writing - original draft, Writing - review & editing. **Bruno Boury:** Writing - review & editing. **Hafida Hentit:** Methodology, Visualization. **Pierre-Emmanuel Lippens:** .

#### CRediT authorship contribution statement

**Meriem Mansour:** Investigation, Methodology. **Bahia Benalioua:** Methodology, Validation. **Abdelhadi Bentouami:** Project administration, Methodology, Writing - original draft, Writing - review & editing. **Bruno Boury:** Analytical equipment, Writing - review & editing. **Hafida Hentit:** Project administration, Methodology, Visualization. **Pierre-Emmanuel Lippens:** Project administration, Provision of analytical equipment.

#### Declaration of Competing Interest

The authors declare that they have no known competing financial interests or personal relationships that could have appeared to influence the work reported in this paper.

#### Acknowledgements

This work is part of a project (A16N01UN270120200005) funded by the thematic science and technology research agency (ATRSDT) of the general direction of scientific research and technological development (DGRSDT) within the Algerian ministry of higher education and scientific research. This work is also part of a TASSILI project (code: 19M-DU205) between the materials recovery laboratory of the University of Mostaganem and the AIME laboratory of the ICGM of the University of Montpellier.

#### Appendix A. Supplementary material

Supplementary data to this article can be found online at <https://doi.org/10.1016/j.apsusc.2020.147577>.

#### References

- [1] H Zhang, H Huang, H Ming, H Li, L Zhang, Y Liu, Z Kang, Carbon quantum dots/Ag<sub>3</sub>PO<sub>4</sub> complex photocatalysts with enhanced photocatalytic activity and stability under visible light, *J. Mater. Chem.* 22 (2012) 10501–10506.
- [2] P Singh, P Sonu, A Raizada, P Sudhaik, P Shandilya, S Thakur, V K Agarwal, Gupta, Enhanced photocatalytic activity and stability of AgBr/BiOBr/graphene heterojunction for phenol degradation under visible light, *J. Saudi Chem. Soc.* 23 (2019) 586–599.
- [3] D Kong, Y Zheng, M Kobielski, Y Wang, Z Bai, W Macyk, X Wang, J Tang, Recent advances in visible light-driven water oxidation and reduction in suspension systems, *Mater. Today* 21 (2018) 897–924.
- [4] X Wang, S Li, H Yu, J Yu, S Liu, Ag<sub>2</sub>O as a new visible-light photocatalyst: self-stability and high photocatalytic activity, *Chem. Eur. J.* 17 (2011) 7777–7780.

- [5] C Tian, Q Zhang, B Jiang, G Tian, H Fu, Glucose-mediated solution–solid route for easy synthesis of Ag/ZnO particles with superior photocatalytic activity and photostability, *J. Alloys Compd.* 509 (2011) 6935–6941.
- [6] Z-D Lei, J-J Wang, L Wang, X-Y Yang, G Xu, L Tang, Efficient photocatalytic degradation of ibuprofen in aqueous solution using novel visible-light responsive graphene quantum dot/AgVO<sub>3</sub> nanoribbons, *J. Hazard. Mater.* 312 (2016) 298–306.
- [7] S Dong, J Feng, M Fan, Y Pi, L Hu, X Han, M Liu, J Sun, J Sun, Recent developments in heterogeneous photocatalytic water treatment using visible light-responsive photocatalysts: a review, *RSC Adv.* 5 (2015) 14610–14630.
- [8] S J A Moniz, S A Shevlin, D J Martin, Z-X Guo, J Tang, Visible-light driven heterojunction photocatalysts for water splitting – a critical review, *Energy Environ. Sci.* 8 (2015) 731–759.
- [9] J Cao, B Xu, H Lin, B Luo, S Chen, Chemical etching preparation of BiOI/BiOBr heterostructures with enhanced photocatalytic properties for organic dye removal, *Chem. Eng. J.* 185–186 (2012) 91–99.
- [10] J Cao, B Xu, B Luo, H Lin, S Chen, Novel BiOI/BiOBr heterojunction photocatalysts with enhanced visible light photocatalytic properties, *Catal. Commun.* 13 (2011) 63–68.
- [11] H Huang, X Han, X Li, S Wang, P K Chu, Y Zhang, Fabrication of multiple heterojunctions with tunable visible-light-active photocatalytic reactivity in BiOBr–BiOI full-range composites based on microstructure modulation and band structures, *ACS Appl. Mater. Interfaces* 7 (2015) 482–492.
- [12] Y Wang, Y Long, Z Yang, D Zhang, A novel ion-exchange strategy for the fabrication of high strong BiOI/BiOBr heterostructure film coated metal wire mesh with tunable visible-light-driven photocatalytic reactivity, *J. Hazard. Mater.* 351 (2018) 11–19.
- [13] S Gao, C Guo, S Hou, L Wan, Q Wang, J Lv, Y Zhang, J Gao, W Meng, J Xu, Photocatalytic removal of tetrabromobisphenol A by magnetically separable flower-like BiOBr/BiOI/Fe<sub>3</sub>O<sub>4</sub> hybrid nanocomposites under visible-light irradiation, *J. Hazard. Mater.* 331 (2017) 1–12.
- [14] H Liu, H Zhou, X Liu, H Li, C Ren, X Li, W Li, Z Lian, M Zhang, Engineering design of hierarchical g-C<sub>3</sub>N<sub>4</sub>@Bi/BiOBr ternary heterojunction with Z-scheme system for efficient visible-light photocatalytic performance, *J. Alloys Compd.* 798 (2019) 741–749.
- [15] D Yuan, L Huang, Y Li, Y Xu, H Xu, S Huang, J Yan, M He, H Li, Synthesis and photocatalytic activity of g-C<sub>3</sub>N<sub>4</sub>/BiOI/BiOBr ternary composites, *RSC Adv.* 6 (2016) 41204–41213.
- [16] C-W Siao, W-L-W Lee, Y-M Dai, W-H Chung, J-T Hung, P-H Huang, W-Y Lin, C-C Chen, BiOxCl<sub>y</sub>/BiOmBrn/BiOpIq/GO quaternary composites: syntheses and application of visible-light-driven photocatalytic activities, *J. Colloid Interface Sci.* 544 (2019) 25–36.
- [17] Y-H Lee, Y-M Dai, J-Y Fu, C-C Chen, A series of bismuth-oxychloride/bismuth-oxynitride/graphene-oxide nanocomposites: synthesis, characterization, and photocatalytic activity and mechanism, *Mol. Catal.* 432 (2017) 196–209.
- [18] X Su, J Yang, X Yu, Y Zhu, Y Zhang, In situ grown hierarchical 50%BiOCl/BiOI hollow flowerlike microspheres on reduced graphene oxide nanosheets for enhanced visible-light photocatalytic degradation of rhodamine B, *Appl. Surf. Sci.* 433 (2018) 502–512.
- [19] E E El-Katori, M A Ahmed, A A El-Bindary, A M Oraby, Impact of CdS/SnO<sub>2</sub> heterostructured nanoparticle as visible light active photocatalyst for the removal methylene blue dye, *J. Photochem. Photobiol., A* 392 (2020) 112403.
- [20] A H Mamaghani, F Haghighat, C-S Lee, Hydrothermal/solvothermal synthesis and treatment of TiO<sub>2</sub> for photocatalytic degradation of air pollutants: preparation, characterization, properties, and performance, *Chemosphere* 219 (2019) 804–825.
- [21] Y Huang, H Xu, H Yang, Y Lin, H Liu, Y Tong, Efficient charges separation using advanced BiOI-based hollow spheres decorated with palladium and manganese dioxide nanoparticles, *ACS Sustain. Chem. Eng.* 6 (2018) 2751–2757.
- [22] I Benyamina, K Manseri, M Mansour, B Benalioua, A Bentouami, B Boury, New Bi<sub>2</sub>O<sub>3</sub>-ZnO composite deposited on glass wool. Effect of the synthesis method on photocatalytic efficiency under visible light, *Appl. Surf. Sci.* 483 (2019) 859–869.
- [23] S Takasugi, K Tomita, M Iwaoka, H Kato, M Kakihana, The hydrothermal and solvothermal synthesis of LiTaO<sub>3</sub> photocatalyst: suppressing the deterioration of the water splitting activity without using a cocatalyst, *Int. J. Hydrogen Energy* 40 (2015) 5638–5643.
- [24] Z Jiang, B Huang, Z Lou, Z Wang, X Meng, Y Liu, X Qin, X Zhang, Y Dai, Immobilization of BiOX (X = Cl, Br) on activated carbon fibers as recycled photocatalysts, *Dalton Trans.* 43 (2014) 8170–8173.
- [25] M Zhang, C Shao, X Zhang, Y Liu, Bismuth oxychloride/carbon nanofiber heterostructures for the degradation of 4-nitrophenol, *CrystEngComm* 17 (2015) 7276–7282.
- [26] B Weng, F Xu, J Xu, Hierarchical structures constructed by BiOX (X = Cl, I) nanosheets on CNTs/carbon composite fibers for improved photocatalytic degradation of methyl orange, *J. Nanopart. Res.* 16 (2014) 2766.
- [27] G Wang, J Wang, P Yang, Composites BiOI nanoplatelets on carbon fibers towards enhanced photocatalysis, *J. Nanosci. Nanotechnol.* 18 (2018) 309–313.
- [28] X Yang, X Wang, Y Zhao, L Xu, T Wang, X Zhang, Preparation of recyclable BiOI/luffa fiber composite and its highly efficient visible light photocatalytic properties, *J. Cleaner Prod.* 200 (2018) 945–953.
- [29] M Yadav, S Garg, A Chandra, K Hernadi, Immobilization of green BiOX (X = Cl, Br and I) photocatalysts on ceramic fibers for enhanced photocatalytic degradation of recalcitrant organic pollutants and efficient regeneration process, *Ceram. Int.* 45 (2019) 17715–17722.
- [30] Y Wang, Q Yang, X Wang, J Yang, Y Dai, Y He, W Chen, W Zhang, Photocatalytic degradation of rhodamine B and diclofenac sodium on hollow hierarchical microspheres of BiOBr modified with sepiolite and polyvinyl pyrrolidone (PVP), *Mater. Sci. Eng. B* 244 (2019) 12–22.
- [31] Y Zhang, G Shan, F Dong, C Wang, L Zhu, Glass fiber supported BiOI thin-film fixed-bed photocatalytic reactor for water decontamination under solar light irradiation, *J. Environ. Sci.* 80 (2019) 277–286.
- [32] M Du, Y Du, Y Feng, Z Li, J Wang, N Jiang, Y Liu, Advanced photocatalytic performance of novel BiOBr/BiOI/cellulose composites for the removal of organic pollutant, *Cellulose* 26 (2019) 5543–5557.
- [33] R Hao, X Xiao, X Zuo, J Nan, W Zhang, Efficient adsorption and visible-light photocatalytic degradation of tetracycline hydrochloride using mesoporous BiOI microspheres, *J. Hazard. Mater.* 209–210 (2012) 137–145.
- [34] X Shi, X Chen, X Chen, S Zhou, S Lou, Y Wang, L Yuan, PVP assisted hydrothermal synthesis of BiOBr hierarchical nanostructures and high photocatalytic capacity, *Chem. Eng. J.* 222 (2013) 120–127.
- [35] K Li, Y Liang, J Yang, Q Gao, Y Zhu, S Liu, R Xu, X Wu, Controllable synthesis of 001 facet dependent foursquare BiOCl nanosheets: a high efficiency photocatalyst for degradation of methyl orange, *J. Alloys Compd.* 695 (2017) 238–249.
- [36] A Malathi, P Arunachalam, J Madhavan, A M Al-Mayouf, M A Ghanem, Rod-on-flake  $\alpha$ -FeOOH/BiOI nanocomposite: facile synthesis, characterization and enhanced photocatalytic performance, *Colloids Surf. A* 537 (2018) 435–445.
- [37] A Phuruangrat, S Thongtem, T Thongtem, Synthesis of hierarchical BiOBr nanostructure flowers by PVP-assisted hydrothermal method and their photocatalytic activities, *J. Electron. Mater.* 48 (2019) 8031–8038.
- [38] L Kong, J Guo, J W Makepeace, T Xiao, H F Greer, W Zhou, Z Jiang, P P Edwards, Rapid synthesis of BiOBr<sub>1-x</sub> photocatalysts: Insights to the visible-light photocatalytic activity and strong deviation from Vegard's law, *Catal. Today* 335 (2019) 477–484.
- [39] J Lu, Q Meng, H Lv, L Shui, M Jin, Z Zhang, Z Chen, M Yuan, X Wang, J-M Liu, G Zhou, Synthesis of visible-light-driven BiOBr<sub>1-x</sub> solid solution nanoplates by ultrasound-assisted hydrolysis method with tunable bandgap and superior photocatalytic activity, *J. Alloys Compd.* 732 (2018) 167–177.
- [40] B Benalioua, M Mansour, A Bentouami, B Boury, E H Elandaloussi, The layered double hydroxide route to Bi-Zn co-doped TiO<sub>2</sub> with high photocatalytic activity under visible light, *J. Hazard. Mater.* 288 (2015) 158–167.
- [41] F-T Li, X-J Wang, Y Zhao, J-X Liu, Y-J Hao, R-H Liu, D-S Zhao, Ionic-liquid-assisted synthesis of high-visible-light-activated N-B-F-tri-doped mesoporous TiO<sub>2</sub> via a microwave route, *Appl. Catal., B* 144 (2014) 442–453.
- [42] L M Pastrana-Martinez, S Morales-Torres, A G Kontos, N G Moustakas, J L Faria, J M Doña-Rodríguez, P Falaras, A M T Silva, TiO<sub>2</sub>, surface modified TiO<sub>2</sub> and graphene oxide-TiO<sub>2</sub> photocatalysts for degradation of water pollutants under near-UV/Vis and visible light, *Chem. Eng. J.* 224 (2013) 17–23.
- [43] L Lin, M Huang, L Long, Z Sun, W Zheng, D Chen, Fabrication of a three-dimensional BiOBr/BiOI photocatalyst with enhanced visible light photocatalytic performance, *Ceram. Int.* 40 (2014) 11493–11501.
- [44] X Zhang, C-Y Wang, L-W Wang, G-X Huang, W-K Wang, H-Q Yu, Fabrication of BiOBr<sub>1-x</sub> photocatalysts with tunable visible light catalytic activity by modulating band structures, *Sci. Rep.* 6 (2016) 22800.
- [45] H Huang, X Li, X Han, N Tian, Y Zhang, T Zhang, Moderate band-gap-broadening induced high separation of electron–hole pairs in Br substituted BiOI: a combined experimental and theoretical investigation, *PCPP* 17 (2015) 3673–3679.
- [46] K K Bera, R Majumdar, M Chakraborty, S K Bhattacharya, Phase control synthesis of  $\alpha$ ,  $\beta$  and  $\alpha/\beta$  Bi<sub>2</sub>O<sub>3</sub> hetero-junction with enhanced and synergistic photocatalytic activity on degradation of toxic dye, Rhodamine-B under natural sunlight, *J. Hazard. Mater.* 352 (2018) 182–191.
- [47] T Jiang, J Li, Y Gao, L Li, T Lu, L Pan, BiOBr/BiOF composites for efficient degradation of rhodamine B and nitrobenzene under visible light irradiation, *J. Colloid Interface Sci.* 490 (2017) 812–818.
- [48] S Zarezadeh, A Habibi-Yangjeh, M Mousavi, S Ghosh, Synthesis of novel p-n-p BiOBr/ZnO/BiOI heterostructures and their efficient photocatalytic performances in removals of dye pollutants under visible light, *J. Photochem. Photobiol., A* 389 (2020) 112247.
- [49] J Li, F Yang, Q Zhou, L Wu, W Li, R Ren, Y Lv, Visible-light photocatalytic performance, recovery and degradation mechanism of ternary magnetic Fe<sub>3</sub>O<sub>4</sub>/BiOBr/BiOI composite, *RSC Adv.* 9 (2019) 23545–23553.
- [50] Y Wang, L Lin, F Li, L Chen, D Chen, C Yang, M Huang, Enhanced photocatalytic bacteriostatic activity towards Escherichia coli using 3D hierarchical microsphere BiOI/BiOBr under visible light irradiation, *Photochem. Photobiol.* 15 (2016) 666–672.
- [51] V Mahmoodi, A Ahmadpour, T R Bastami, M T H Mosavian, PVP assisted synthesis of high efficient BiOI/Graphene oxide nanohybrid and its photocatalytic performance in degradation of organic dye pollutants, *Sol. Energy* 176 (2018) 483–495.
- [52] J Yang, T Xie, Q Zhu, J Wang, L Xu, C Liu, Boosting the photocatalytic activity of BiOX under solar light via selective crystal facet growth, *J. Mater. Chem. C* 8 (2020) 2579–2588.
- [53] C Chang, H-C Yang, N Gao, S-Y Lu, Core/shell p-BiOI/n- $\beta$ -Bi<sub>2</sub>O<sub>3</sub> heterojunction array with significantly enhanced photoelectrochemical water splitting efficiency, *J. Alloys Compd.* 738 (2018) 138–144.
- [54] H Qin, K Wang, L Jiang, J Li, X Wu, G Zhang, Ultrasonic-assisted fabrication of a direct Z-scheme BiOI/Bi<sub>2</sub>O<sub>4</sub> heterojunction with superior visible light-responsive photocatalytic performance, *J. Alloys Compd.* 821 (2020) 153417.
- [55] L Cai, J Yao, J Li, Y Zhang, Y Wei, Sonochemical synthesis of BiOI-TiO<sub>2</sub> heterojunction with enhanced visible-light-driven photocatalytic activity, *J. Alloys Compd.* 783 (2019) 300–309.
- [56] Y Huang, W Wang, Q Zhang, J-J Cao, R-J Huang, W Ho, S C Lee, In situ fabrication of  $\alpha$ -Bi<sub>2</sub>O<sub>3</sub>/(BiO)<sub>2</sub>CO<sub>3</sub> nanoplate heterojunctions with tunable optical property and photocatalytic activity, *Sci. Rep.* 6 (2016) 23435.
- [57] N Zhang, D Chen, F Niu, S Wang, L Qin, Y Huang, Enhanced visible light photocatalytic activity of Gd-doped BiFeO<sub>3</sub> nanoparticles and mechanism insight, *Sci. Rep.* 6 (2016) 26467.
- [58] J Hou, K Jiang, M Shen, R Wei, X Wu, F Idrees, C Cao, Micro and nano hierarchical structures of BiOI/activated carbon for efficient visible-light-photocatalytic reactions, *Sci. Rep.* 7 (2017) 11665.

- [59] S Han, J Li, K Yang, J Lin, Fabrication of a  $\beta$ -Bi<sub>2</sub>O<sub>3</sub>/BiOI heterojunction and its efficient photocatalysis for organic dye removal, *Chin. J. Catal.* 36 (2015) 2119–2126.
- [60] R López, R Gómez, Band-gap energy estimation from diffuse reflectance measurements on sol-gel and commercial TiO<sub>2</sub>: a comparative study, *J. Sol-Gel Sci. Technol.* 61 (2012) 1–7.
- [61] H Lin, C P Huang, W Li, C Ni, S I Shah, Y-H Tseng, Size dependency of nanocrystalline TiO<sub>2</sub> on its optical property and photocatalytic reactivity exemplified by 2-chlorophenol, *Appl. Catal., B* 68 (2006) 1–11.
- [62] J Aguado, R van Grieken, M-J López-Muñoz, J Marugán, A comprehensive study of the synthesis, characterization and activity of TiO<sub>2</sub> and mixed TiO<sub>2</sub>/SiO<sub>2</sub> photocatalysts, *Appl. Catal., A* 312 (2006) 202–212.
- [63] R R Yeredla, H Xu, An investigation of nanostructured rutile and anatase plates for improving the photosplitting of water, *Nanotechnology* 19 (2008) 055706.
- [64] N Sangiorgi, L Aversa, R Tatti, R Verucchi, A Sanson, Spectrophotometric method for optical band gap and electronic transitions determination of semiconductor materials, *Opt. Mater.* 64 (2017) 18–25.
- [65] X Zhang, Z Ai, F Jia, L Zhang, Generalized one-pot synthesis, characterization, and photocatalytic activity of hierarchical BiOX (X = Cl, Br, I) nanoplate microspheres, *J. Phys. Chem. C* 112 (2008) 747–753.
- [66] Y Lei, G Wang, S Song, W Fan, M Pang, J Tang, H Zhang, Room temperature, template-free synthesis of BiOI hierarchical structures: visible-light photocatalytic and electrochemical hydrogen storage properties, *Dalton Trans.* 39 (2010) 3273–3278.
- [67] J Li, Q Zhou, F Yang, L Wu, W Li, R Ren, Y Lv, Uniform flower-like BiOBr/BiOI prepared by a new method: visible-light photocatalytic degradation, influencing factors and degradation mechanism, *New J. Chem.* 43 (2019) 14829–14840.
- [68] K Yu, S Yang, H He, C Sun, C Gu, Y Ju, Visible light-driven photocatalytic degradation of rhodamine B over NaBiO<sub>3</sub>: pathways and mechanism, *J. Phys. Chem. A* 113 (2009) 10024–10032.
- [69] P Wang, M Cheng, Z Zhang, On different photodecomposition behaviors of rhodamine B on laponite and montmorillonite clay under visible light irradiation, *J. Saudi Chem. Soc.* 18 (2014) 308–316.
- [70] C Lops, A Ancona, K Di Cesare, B Dumontel, N Garino, G Canavese, S Hernández, V Cauda, Sonophotocatalytic degradation mechanisms of Rhodamine B dye via radicals generation by micro- and nano-particles of ZnO, *Appl. Catal., B* 243 (2019) 629–640.
- [71] K V Kumar, K Porkodi, F Rocha, Langmuir-Hinshelwood kinetics – a theoretical study, *Catal. Commun.* 9 (2008) 82–84.
- [72] J Liu, X Li, R Li, Q Zhao, J Ke, H Xiao, L Wang, S Liu, M Tade, S Wang, Facile synthesis of tube-shaped Mn-Ni-Ti solid solution and preferable Langmuir-Hinshelwood mechanism for selective catalytic reduction of NO<sub>x</sub> by NH<sub>3</sub>, *Appl. Catal., A* 549 (2018) 289–301.
- [73] H Ji, F Chang, X Hu, W Qin, J Shen, Photocatalytic degradation of 2,4,6-trichlorophenol over g-C<sub>3</sub>N<sub>4</sub> under visible light irradiation, *Chem. Eng. J.* 218 (2013) 183–190.
- [74] A Walsh, K T Butler, Prediction of electron energies in metal oxides, *Acc. Chem. Res.* 47 (2014) 364–372.
- [75] R S Mulliken, A new electroaffinity scale together with data on valence states and on valence ionization potentials and electron affinities, *J. Chem. Phys.* 2 (1934) 782–793.
- [76] Y Wang, J Sunarso, B Zhao, C Ge, G Chen, One-dimensional BiOBr nanosheets/TiO<sub>2</sub> nanofibers composite: controllable synthesis and enhanced visible photocatalytic activity, *Ceram. Int.* 43 (2017) 15769–15776.
- [77] Y Li, J Wang, H Yao, L Dang, Z Li, Chemical etching preparation of BiOI/Bi<sub>2</sub>O<sub>3</sub> heterostructures with enhanced photocatalytic activities, *Catal. Commun.* 12 (2011) 660–664.
- [78] S P Pattnaik, A Behera, S Marthia, R Acharya, K Parida, Facile synthesis of exfoliated graphitic carbon nitride for photocatalytic degradation of ciprofloxacin under solar irradiation, *J. Mater. Sci.* 54 (2019) 5726–5742.
- [79] A Behera, D Kandi, S Mansingh, S Marthia, K Parida, Facile synthesis of ZnFe<sub>2</sub>O<sub>4</sub>@RGO nanocomposites towards photocatalytic ciprofloxacin degradation and H<sub>2</sub> energy production, *J. Colloid Interface Sci.* 556 (2019) 667–679.
- [80] S Hu, J Zhu, L Wu, X Wang, P Liu, Y Zhang, Z Li, Effect of fluorination on photocatalytic degradation of rhodamine B over In(OH)<sub>3</sub>Sz: promotion or suppression?, *J. Phys. Chem. C* 115 (2011) 460–467.